

NUMERICAL MULTISCALE METHODS AND EFFECTIVE BOUNDARY CONDITIONS *

SEAN P. CARNEY[†] AND BJÖRN ENGQUIST^{†‡}

Abstract. We develop numerical multiscale methods for viscous boundary layer flow. The goal is to derive effective boundary conditions, or wall laws, through high resolution simulations localized to the boundary coupled to a coarser simulation in the domain interior. The multiscale framework is analyzed in the context of laminar flow over a rough boundary. Asymptotic analysis shows that, up to a small perturbation, the method recovers the slip constant in the wall law derived from periodic homogenization theory. Numerical experiments illustrate the utility of the method for more general roughness patterns and fair field flow conditions.

1. Introduction. Standard partial differential equations for viscous flow such as the Stokes and Navier-Stokes equations naturally have no slip boundary conditions. The velocity vector $u = 0$ at the boundary.

There are cases where this is not accurate. At a slip line where two immiscible fluids meet at a solid boundary is one example [15]. The fluid molecules actually slide along the boundary near the slip line. Another example is gas at very low pressure.

Even when the no slip boundary condition is valid, it can generate an asymptotic separation of energetic scales, manifest in the form of boundary layers. Such boundary layer flows are challenging both for analysis and numerical computation. Some examples include high Reynolds number wall bounded flows, electro-kinetic flows over charged surfaces, and viscous flow over a rough surface or a porous bed.

In such cases, it may be better in a computation to replace the no slip boundary condition by an effective boundary condition, or wall law. Ideally, the wall law captures the effect of the asymptotic small scales on the large scales. Computing in a domain without the small scale structure then results in a large reduction in the degrees of freedom necessary in a simulation. Sometimes wall laws can be rigorously derived from first principles; examples include the Navier-slip law for flows over a rough surface [27] and the Beavers-Joseph-Saffman interface law for flows over porous beds [26]. In other cases one has to resort to physical intuition or engineering wisdom in order to derive effective boundary conditions. Classical examples include the logarithmic law-of-the-wall [36] and the electro-osmotic slip velocity (and associated zeta potential) [39] for wall bounded turbulent and electro-kinetic flows, respectively.

The focus here will be on laminar flow with a rough boundary that varies with characteristic amplitude and period $0 < \epsilon \ll 1$. Surface roughness plays an important role in a variety of physical applications, such as in geophysical fluid dynamics [10, 37] or in the reduction of skin friction drag. The morphology of a swordfish's sword, shark dermal denticles, and riblets on the Stars and Stripes yacht in the 1987 America's Cup finals are all examples of the latter [11, 35]. The problem is also well understood mathematically [4, 6, 9, 13, 27].

The basic goal is to model the effect of the rough boundary on the flow in the domain interior and thus remove the ϵ -scale from the problem. Computational techniques based on domain decomposition and asymptotic homogenization theory have been previously proposed for this purpose [4, 5]. Similar strategies have also been

*

Funding: This research is supported by National Science Foundation Grant DMS-1620396.

[†]Department of Mathematics, University of Texas at Austin

[‡]Oden Institute for Computational Engineering and Sciences, University of Texas at Austin

explored for compressible flows over rough surfaces [14] and for shape optimization with the purpose of minimizing drag for both laminar and turbulent incompressible flows, assuming the roughness is within the viscous sublayer [19, 20].

Our goal is to derive the Navier-slip effective boundary condition by a local high-resolution simulation coupled to the coarser scale simulation in the interior following the framework of the heterogeneous multiscale method (HMM) [1, 16, 17]. This coarser scale simulation will use the effective boundary condition.

The HMM framework has been applied to the slip line problem mentioned above. The local high-resolution model is then molecular dynamics. The outer coarser scale model is the Navier-Stokes equations, which gets an effective boundary condition at the slip line from the molecular dynamics simulation, [38, 17].

The method proposed here for laminar flow over a rough boundary is similar to domain decomposition, but it uses the Robin-type boundary condition from the mathematical homogenization theory. In the academic setting of periodic roughness, it is designed to reproduce the slip amount from the theory. However, no assumption of local flow periodicity is made, in contrast to [5], and hence the coupling procedure can work in more general settings.

The structure of the paper is as follows. The heterogeneous multiscale method is briefly described in section 2 since it will be used in the description of the numerical methods presented below. The problem of laminar, viscous flow over a rough boundary is introduced in section 3. Since the analysis of the multiscale method introduced in section 4 relies on the asymptotic expansions performed in [4], the analysis is repeated in a slightly more general setting. Lastly, numerical results in section 5 illustrate not only that the method reproduces the theoretical wall law predicted from the homogenization theory when applicable, but that it also performs well in more general settings.

2. The heterogeneous multiscale method. The heterogeneous multiscale method (HMM) is a general framework for designing multiscale algorithms that aims to capture the macroscopic behavior of a system without resolving the microscopic details in their entirety. Under the assumption of scale separation in the underlying physical system, HMM couples macroscopic simulations to local, microscopic simulations so that the simulation has an overall computational complexity independent of the fine scale. Comprehensive introductions to and reviews of HMM can be found in [1, 16, 17]; below we briefly describe the main idea of the method and its applicability to designing effective boundary conditions for fluid simulations.

Suppose there is a general model for the macroscopic state of a physical system that can be expressed as $M(\Psi, D) = 0$, where D represents the macroscopic data necessary for the model to be complete. Then the main goal of HMM is to approximate D by solving microscale problems locally in space and/or time that are constrained by the macroscopic solution. If the microscale problem is denoted by $m(\psi, d) = 0$, where the data d represents the input from the macroscopic system, then the HMM can be succinctly expressed as

$$(2.1) \quad \begin{aligned} M(\Psi, D) &= 0, & D &= D(\psi) \\ m(\psi, d) &= 0, & d &= d(\Psi). \end{aligned}$$

With a macroscopic solver in hand, the procedure is to first constrain the micro simulation to be consistent with local macro data: $d = d(\Psi)$. After solving for ψ in the micro domain, the missing macro data is estimated using the results from the micro simulation: $D = D(\psi)$.

As mentioned in the introduction, the HMM framework has been applied to fluid simulation problems before. For instance, in [38], the authors model fluid-fluid and fluid-solid interactions in which the standard boundary conditions for a continuum fluid are no longer accurate and must be inferred from microscopic models, such as molecular dynamics (MD). Using such a microscopic model throughout the entire computational domain is prohibitively expensive, due to the disparate spatial and temporal scales between the continuum and molecular dynamics involved. Instead, local molecular dynamic simulations are computed only along the interfaces for which a boundary condition is needed. In the language of (2.1) above, the model is

$$(2.2) \quad M(\Psi, D) = \begin{cases} \rho \mathbf{u}_t + \nabla \cdot \tau = 0, & \tau = \tau(\mathbf{q}_i, \mathbf{p}_i) \\ \nabla \cdot \mathbf{u} = 0 \end{cases}$$

$$(2.3) \quad m(\psi, d) = \begin{cases} m_i \frac{d}{dt} \mathbf{q}_i = \mathbf{p}_i \\ \frac{d}{dt} \mathbf{p}_i = \mathbf{F}_i, & \mathbf{p}_i(t=0) = \mathbf{p}_i(\mathbf{u}), \end{cases}$$

the point being that the usual stress tensor

$$(2.4) \quad \tau = \rho \mathbf{u} \otimes \mathbf{u} + pI + \tau_d, \quad \tau_d = \mu (\nabla \mathbf{u} + \nabla \mathbf{u}^T)$$

can be replaced with a more accurate model coming from the MD simulation where it is needed, and the MD simulation is initialized to be consistent with the local values of the continuum velocity.

While not initially proposed as an example of HMM, the method of Superparameterization proposed by Grabowski [23] and developed by Majda and others [32, 33, 24, 34] is a multiscale method for the simulation of atmospheric flows that fits into the framework of HMM. The original idea of the method is to couple local computations for the turbulent transport quantities to a global macroscopic model for the atmosphere. The local computations impose artificial scale separation in both space and time between the large scale energetic motions and the small scale fluctuations and hence allow for a reduced computational cost.

We mention also recent work for determining the effective boundary condition at the interface between a free fluid and a porous medium [28]. The method fits in the HMM framework and is quite similar to the one proposed in this work; the coefficients in a generalized Beavers-Joseph law are determined by solving Stokes problems in a microscale domain containing a unit cell of the porous media.

In the present setting of viscous laminar flow over a rough boundary, the macroscopic model M consists of the Navier-Stokes equations posed in domain with a smooth boundary. The missing data D necessary for the model to be complete is the coefficient in the wall law coming from the homogenization theory. The microscopic model m consists again of the Navier-Stokes equations, this time posed on a single “element” of roughness whose size is finite in the wall-normal direction (in contrast to the linear cell problem from the homogenization theory, which is posed on a semi-infinite domain, as discussed below). The constraint d is that the values of the microscopic solution variables ψ at the computational boundaries (those that are *not* the rough wall, where the no slip condition is prescribed) must be consistent with the local values of the macroscopic flow variables Ψ at those locations. Once the microscopic problem is solved, the solution ψ is suitably averaged to estimate D ; in this way the models are formally coupled.

3. Homogenization theory for laminar flow over rough boundary. There exists a large amount of mathematical results available in the literature concerning

the asymptotic behavior of laminar incompressible flow in the presence of a rough boundary; see [2, 3, 4, 8, 6, 9, 13, 27], and references therein. Although there are differing physical assumptions and levels of mathematical rigour associated to each work, all justify the use of a Robin-type condition on a smooth boundary near the original rough boundary. The slip constant α in the wall law

$$(3.1) \quad u = \alpha \frac{\partial u}{\partial n}$$

(where n is the unit vector normal to the smooth boundary) depends on the average of a local corrector that decays exponentially in the fast variable. As noted above, the removal of the ϵ -scale of the problem is of practical use, as the number of mesh nodes in a numerical simulation that would be needed for a full treatment of the problem is drastically reduced.

Below we give some preliminary definitions necessary to describe two-dimensional viscous, laminar flow in a rough domain. Since the asymptotic analysis of [4] is used for the convergence analysis of the multiscale algorithm presented in section 4, it is reproduced below in a slightly more general setting—namely that of periodic roughness that is modulated by a smooth function.

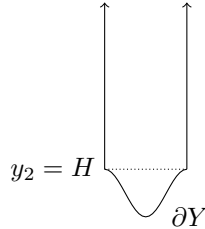


FIG. 1. Semi-infinite domain Y with boundary $\partial Y = \{y \in \mathbb{R}^2 | y_2 = \varphi(y_1)\}$ for some periodic function φ .

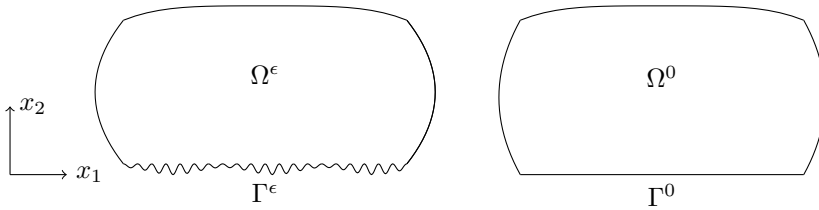


FIG. 2. Domain Ω^ϵ with periodic, sinusoidal roughness modulated by a smooth function.

3.1. Preliminary definitions. Let $\varphi : \mathbb{R} \rightarrow \mathbb{R}$ be a bounded, Lipschitz continuous, periodic function with maximum value $H := \|\varphi\|_\infty$ that satisfies $\varphi(N) = H$ for every $N \in \mathbb{Z}$, and $\varphi(y+1) = \varphi(y) \geq 0 \forall y \in \mathbb{R}$. Let ϵ be some fixed small parameter, $0 < \epsilon \ll 1$, and define $\varphi^\epsilon(x_1) := \epsilon\varphi(x_1/\epsilon)$. For smooth, bounded function $\beta : \mathbb{R} \rightarrow \mathbb{R}$ that is independent of ϵ , define $\zeta^\epsilon(x_1) := \beta(x_1)\varphi^\epsilon(x_1)$ to be the function that parameterizes the rough boundary. Without loss of generality, assume that $\|\beta\|_\infty = 1$ for ease of exposition below. Further assume that $\beta \geq 0$ so that $\zeta^\epsilon(x_1) \geq 0 \forall x_1 \in \mathbb{R}$.

Let $Y = \{(y_1, y_2) \in [0, 1) \times \mathbb{R} | y_2 \geq \varphi(y_1)\}$ be a domain containing a periodic “cell” of φ , semi-infinite in the vertical direction with boundary $\partial Y = \{y \in \mathbb{R}^2 | y_2 = \varphi(y_1)\}$; for example, see figure 1.

Let $\Theta^\epsilon = \{(x_1, x_2) \in \mathbb{R}^2 \mid x_2 \geq \zeta^\epsilon(x_1)\}$ be the semi-infinite domain contained in the upper half plane $x_2 \geq 0$ in \mathbb{R}^2 , and let Ω be a bounded domain in \mathbb{R}^2 made of one piece that intersects the line $\{x_2 = 0\}$. Take $\Omega^0 = \Omega \cap \{x_2 > 0\}$, and let $\Gamma^0 = \partial\Omega^0 \cap \{x_2 \geq 0\}$. Finally, take $\Omega^\epsilon := \Theta^\epsilon \cap \Omega^0$, so that Ω^ϵ has a rough boundary Γ^ϵ with characteristic amplitude and wavelength ϵ ; for example, see figure 2. Note that $\overline{\Omega^\epsilon} \rightarrow \overline{\Omega^0}$ as $\epsilon \rightarrow 0$.

3.2. Asymptotic analysis. With Ω^ϵ in hand, consider the following stationary Navier-Stokes problem

$$(3.2) \quad \begin{aligned} \mathcal{L}(u^\epsilon, p^\epsilon) &:= u^\epsilon \nabla u^\epsilon - \nu \Delta u^\epsilon + \nabla p^\epsilon = f && \text{in } \Omega^\epsilon \\ \nabla \cdot u^\epsilon &= 0 && \text{in } \Omega^\epsilon \\ u^\epsilon &= 0 && \text{on } \partial\Omega^\epsilon. \end{aligned}$$

Note that other combinations of well-posed boundary conditions are possible, so long as the no slip condition $u^\epsilon = 0$ is imposed on the rough wall Γ^ϵ .

The authors in [4] consider the regime of high Reynolds number, laminar stationary flow; in this case, the flow exhibits Prandtl boundary layers of characteristic size $\mathcal{O}(\sqrt{\nu})$ [12]. Assuming $|\Omega^0| = \mathcal{O}(1)$, they hypothesize that the effects of surface roughness on the mean flow will be contained in the boundary layer when

$$(3.3) \quad \epsilon \ll \sqrt{\nu}.$$

For simplicity of the asymptotic analysis, the authors take $\nu = \mu\epsilon$, $\mu = \mathcal{O}(1)$, which we consider in this section as well. For other choices of ν that still satisfy (3.3), different asymptotic expansions must be considered. As in [4], we take $\nu = \mu\epsilon$ and assume the system (3.2) has a unique smooth solution.

The goal of the asymptotic analysis is to derive an effective boundary condition similar to (3.1). The starting point is to search for approximations to (u^ϵ, p^ϵ) of the form

$$(3.4) \quad u^\epsilon \approx u^0(x) + \epsilon u_{BL}^1(x, x/\epsilon)$$

$$(3.5) \quad p^\epsilon \approx p^0(x) + \epsilon p_{BL}^1(x, x/\epsilon),$$

where (u^0, p^0) satisfy

$$(3.6) \quad \begin{aligned} \mathcal{L}(u^0, p^0) &= f && \text{in } \Omega^0 \\ \nabla \cdot u^0 &= 0 && \text{in } \Omega^0 \\ u^0 &= 0 && \text{on } \partial\Omega^0, \end{aligned}$$

and (u_{BL}^1, p_{BL}^1) are boundary layer correctors.

Consider first the error that arises when u^0 does *not* satisfy the no slip condition along the rough boundary Γ^ϵ . For $x^0 \in \Gamma^0$, $x^0 + \zeta^\epsilon(x_1^0)e_2 \in \Gamma^\epsilon$, a Taylor expansion and the no slip condition give

$$(3.7) \quad \begin{aligned} u^0(x^0 + \zeta^\epsilon(x_1^0)e_2) &= \overbrace{u^0(x^0)}^{=0} + \zeta^\epsilon(x_1^0) \frac{\partial u^0}{\partial x_2}(x^0) + \frac{1}{2} (\zeta^\epsilon(x_1^0))^2 \frac{\partial^2 u^0}{\partial x_2^2}(x^0) \\ &= \epsilon \beta(x_1^0) \varphi(x_1^0/\epsilon) \frac{\partial u^0}{\partial x_2}(x^0) + \mathcal{O}(\epsilon^2), \end{aligned}$$

so that to leading order in ϵ , the error on the rough boundary Γ^ϵ is given as the product of a function of the macroscopic, “slow” variable x^0

$$(3.8) \quad \beta(x_1^0) \frac{\partial u^0}{\partial x_2}(x^0)$$

and a periodic function of the microscopic, “fast” variable x^0/ϵ

$$(3.9) \quad \varphi(x_1^0/\epsilon).$$

Since the no-slip condition implies $\partial u_1^0/\partial x_1 = 0$ along the smooth wall Γ^0 , the continuity equation implies

$$(3.10) \quad \frac{\partial u^0}{\partial x_2}(x^0) = \frac{\partial u_1^0}{\partial x_2}(x^0) e_1, \quad x^0 \in \Gamma^0.$$

This motivates an ansatz for the boundary layer correctors of the form

$$(3.11) \quad u_{BL}^1(x, y) = \beta(x_1) \frac{\partial u_1^0}{\partial x_2}(x_1, 0) (\chi(y) - \bar{\chi})$$

$$(3.12) \quad p_{BL}^1(x, y) = \beta(x_1) \frac{\partial u_1^0}{\partial x_2}(x_1, 0) \pi(y)$$

where $x = (x_1, x_2)$, χ is a periodic function of $y := x/\epsilon$, and $\bar{\chi}$ is a constant vector. Using the formal differentiation rule

$$(3.13) \quad \nabla \Phi(x, x/\epsilon) = \nabla_x \Phi(x, y) + \frac{1}{\epsilon} \nabla_y \Phi(x, y),$$

inserting (3.4) and (3.5) into \mathcal{L} , and grouping together terms of similar asymptotic order gives

$$(3.14)$$

$$\mathcal{L}(u^0 + \epsilon u_{BL}^1, p^0 + \epsilon p_{BL}^1) - f = \mathcal{L}(u^0, p^0) - f + \beta(x_1) \frac{\partial u_1^0}{\partial x_2}(x_1, 0) (-\mu \Delta_y \chi + \nabla_y \pi)$$

$$(3.15) \quad + \beta(x_1) \frac{\partial u_1^0}{\partial x_2} u^0 \cdot \nabla_y \chi + \mathcal{O}(\epsilon)$$

$$(3.16) \quad = \beta(x_1) \frac{\partial u_1^0}{\partial x_2}(x_1, 0) (-\mu \Delta_y \chi + \nabla_y \pi) + \mathcal{O}(\epsilon^{1/2}).$$

The term in (3.15) is $\mathcal{O}(\epsilon^{1/2})$ or smaller throughout Ω^0 because (i) u^0 is $\mathcal{O}(\epsilon)$ near Γ^0 , (ii) $\nabla_y \chi$ decays exponentially fast as x_2/ϵ grows, as guaranteed a posteriori by [Theorem 3.1](#), and (iii) by assumption of the Prandtl boundary layer scales, $\partial u_1^0/\partial x_2 = \mathcal{O}(\nu^{-1/2}) = \mathcal{O}(\epsilon^{-1/2})$. Hence, if (χ, π) are chosen such that

$$(3.17) \quad -\mu \Delta_y \chi + \nabla_y \pi = 0,$$

then the approximations (3.4) and (3.5) will be $\mathcal{O}(\epsilon^{1/2})$ pointwise in Ω^0 . A similar computation gives

$$(3.18) \quad \nabla \cdot (u^0 + \epsilon u_{BL}^1) = \beta(x_1) \frac{\partial u_1^0}{\partial x_2}(x_1, 0) \nabla_y \cdot \chi + \mathcal{O}(\epsilon)$$

which implies χ should be made divergence free:

$$(3.19) \quad \nabla_y \cdot \chi = 0.$$

Lastly, consider again the pointwise error on the rough boundary $x = x^0 + \zeta^\epsilon(x_1^0)e_2 \in \Gamma^\epsilon$. In contrast to (3.7), the error on Γ^ϵ for the approximation (3.4) is:

$$(3.20) \quad \begin{aligned} u^0(x) + \epsilon u_{BL}^1(x, x/\epsilon) &= \epsilon\beta(x_1^0) \left(\varphi(x_1^0/\epsilon) \frac{\partial u_1^0}{\partial x_2}(x_1^0, 0) e_1 + \frac{\partial u_1^0}{\partial x_2}(x_1, 0) (\chi(x/\epsilon) - \bar{\chi}) \right) \\ &\quad + \mathcal{O}(\epsilon^2) \end{aligned}$$

(note $x_1 = x_1^0$). Hence, one could enforce the boundary condition

$$(3.21) \quad \chi(x/\epsilon) - \bar{\chi} = -\varphi(x_1/\epsilon) e_1, \quad x \in \Gamma^\epsilon$$

in order to eliminate the $\mathcal{O}(\epsilon)$ error terms. The resulting problem for (χ, π) in the periodic cell Y becomes

$$(3.22) \quad \begin{aligned} -\mu \Delta_y \chi + \nabla_y \pi &= 0 && \text{in } Y \\ \nabla_y \cdot \chi &= 0 && \text{in } Y \\ \chi(y) - \bar{\chi} &= -\varphi(y_1) && y \in \partial Y \\ \chi - \bar{\chi} &\in H_{\text{per}}^1(Y) \\ \pi &\in L_{\text{per}}^2(Y). \end{aligned}$$

It can be shown, however, that in general the problem (3.22) has no solutions. Borrowing an example from [4], simply take $\varphi(y_1) = C > 0$. Instead, the Dirichlet condition in (3.22) can be modified so that only

$$(3.23) \quad \chi(y) = -\varphi(y_1), \quad y \in \partial Y$$

is enforced. In order to ensure that (3.4) is $\mathcal{O}(\epsilon^2)$ on Γ^ϵ , replace (u^0, p^0) with (u^1, p^1) , where u^1 satisfies

$$(3.24) \quad u^1(x^0) = \epsilon\beta(x_1^0) \bar{\chi} \frac{\partial u_1^1}{\partial x_2}(x^0), \quad x^0 \in \Gamma^0.$$

This is exactly the desired effective boundary condition, or wall law, of the form (3.1). Accordingly, the $\partial u_1^0/\partial x_2(x_1, 0)$ term in boundary layer correctors (3.11) and (3.12) must be replaced with $\partial u_1^1/\partial x_2(x_1, 0)$; the analysis above, however, is unchanged since both expressions are $\mathcal{O}(\nu^{-1/2})$ near Γ^0 , and hence asymptotically equivalent.

In summary, the approximations

$$(3.25) \quad \begin{aligned} u^\epsilon(x) &\approx u^1(x) + \epsilon\beta(x_1) \frac{\partial u_1^1}{\partial x_2}(x_1, 0) (\chi(x/\epsilon) - \bar{\chi}) \\ p^\epsilon(x) &\approx p^1(x) + \epsilon\beta(x_1) \frac{\partial u_1^1}{\partial x_2}(x_1, 0) \pi(x/\epsilon), \end{aligned}$$

where (u^1, p^1) satisfy

$$(3.26) \quad \begin{aligned} \mathcal{L}(u^1, p^1) &= f && \text{in } \Omega^0 \\ \nabla \cdot u^1 &= 0 && \text{in } \Omega^0 \\ u^1(x) - \epsilon\beta(x_1) \bar{\chi} \frac{\partial u_1^1}{\partial x_2}(x) &= 0 && x \in \Gamma^0 \\ u^1 &= 0 && \text{on } \partial\Omega^0 \setminus \Gamma^0 \end{aligned}$$

and (χ^1, π^1) satisfy

$$(3.27) \quad \begin{aligned} -\mu \Delta_y \chi + \nabla_y \pi &= 0 && \text{in } Y \\ \nabla_y \cdot \chi &= 0 && \text{in } Y \\ \chi(y) &= -\varphi(y_1) && y \in \partial Y \\ \chi - \bar{\chi} &\in H_{\text{per}}^1(Y) \\ \pi &\in L_{\text{per}}^2(Y). \end{aligned}$$

are $\mathcal{O}(\epsilon^{1/2})$ in Ω^0 and $\mathcal{O}(\epsilon^2)$ on Γ^0 . In the linear (Stokes) case, it has been shown that the above approximations are one order (in $\epsilon^{1/2}$) better than (u^0, p^0) ; similar results have also been obtained for Maxwell's equations in a rough domain—see [2, 3, 8].

The following two theorems are due to Achdou et al. The first gives rigorous backing to the assertion that the local correctors (u_{BL}^1, p_{BL}^1) decay exponentially fast in the fast variable x/ϵ , so that the term (3.15) resulting from the insertion of the asymptotic expansions (3.4) and (3.5) into \mathcal{L} is indeed $\mathcal{O}(\epsilon^{1/2})$.

THEOREM 3.1. [4] *Let $\mathcal{S}_{\text{per}}(Y)$ denote the space of all functions in Y that decay exponentially fast in y_2 , as well all of their derivatives, and are 1-periodic in y_1 . Then there exists a unique pair of functions (χ, π) and a unique vector $\bar{\chi} \in \mathbb{R}^2$ such that $\chi - \bar{\chi} \in (H_{\text{per}}^1(Y))^2 \cap (\mathcal{S}_{\text{per}}(Y))^2$, $\pi \in L_{\text{per}}^2(Y) \cap \mathcal{S}_{\text{per}}(Y)$ and (3.27) is satisfied in a weak sense. Furthermore, $\bar{\chi}$ is horizontal,*

$$(3.28) \quad \bar{\chi} = |\bar{\chi}| e_1.$$

Note [Theorem 3.1](#) also ensures the wall law (3.24) is of slip and no-penetration type for the horizontal and vertical component of u^1 , respectively. The second theorem provides a bound on the size of the constant $-\bar{\chi}$ and is crucial for the well posedness of the effective problem (3.26) and hence for its numerical approximation as well.

THEOREM 3.2. [4] *Let $H := \max_{y \in \partial Y} y = \|\varphi\|_\infty$. Then the constant $-\bar{\chi}$ satisfies the bound*

$$0 \leq -\bar{\chi} \leq H.$$

As a result, the problem (3.26) is ill-posed; its variational form contains the term

$$(3.29) \quad \frac{\mu}{\beta \bar{\chi}} \int_{\Gamma^0} u_1^1 v_1 ds$$

where v is a test function, which is not coercive when $\bar{\chi} < 0$. For this reason, the effective problem is instead

$$(3.30) \quad \begin{aligned} \mathcal{L}(u^1, p^1) &= f && \text{in } \Omega_{\epsilon H}^0 \\ \nabla \cdot u^1 &= 0 && \text{in } \Omega_{\epsilon H}^0 \\ u^1(x) - \epsilon \beta(x_1)(\bar{\chi} + H) \frac{\partial u_1^1}{\partial x_2}(x) &= 0 && x \in \Gamma_{\epsilon H}^0 \\ u^1 &= 0 && \text{on } \partial \Omega^0 \setminus \Gamma_{\epsilon H}^0, \end{aligned}$$

where

$$(3.31) \quad \Omega_{\epsilon H}^0 = \Omega^0 \cap \{x_2 \geq \epsilon H\}, \quad \Gamma_{\epsilon H}^0 = \{x + (0, \epsilon H), x \in \Gamma^0\},$$

so that $\Omega_{\epsilon H}^0 \subset \Omega^\epsilon \subset \Omega^0$. A Taylor expansion of the effective boundary condition (3.24) implies that the approximation

$$(3.32) \quad u^1(x) + \epsilon\beta(x_1) \frac{\partial u_1^1}{\partial x_2}(x_1, \epsilon H) (\chi(x/\epsilon) - \bar{\chi}) = \mathcal{O}(\epsilon^2), \quad x \in \Gamma_{\epsilon H}^0$$

still holds.

In conclusion, when discussing the convergence of the multiscale scheme in section 4 below, the desired target, homogenized solution is the one satisfying (3.30).

4. Heterogeneous multiscale method for laminar flow over a rough boundary. We now describe a heterogeneous multiscale method (HMM) for the efficient computation of the effective boundary condition, or wall law, for the case of laminar flow over a rough surface. After some preliminary definitions, the multiscale model is introduced before an algorithm for its practical solution is described. Analysis of the algorithm in the setting of periodic roughness then demonstrates the method's convergence to the homogenized solution from [4] described in section 3.

Consider a translation of the domains Ω^ϵ and $\Omega_{\epsilon H}^0$ defined in subsection 3.1 and (3.31) by ϵH units in the negative x_2 direction, where $H = \|\varphi\|_\infty$ as before, so that

$$(4.1) \quad (x_1, x_2) \mapsto (x_1, x_2 - \epsilon H);$$

note that $\Omega_{\epsilon H}^0 \subset \Omega^\epsilon$ still holds after the translation. Define Ω^{mac} to be the resulting translation of $\Omega_{\epsilon H}^0$, and for simplicity continue to refer to the translation of Ω^ϵ as Ω^ϵ (and similarly for Γ^ϵ). In addition, rename $\Gamma_{\epsilon H}^0$ —the flat part of the boundary of Ω^{mac} defined by (3.31)—to be simply Γ .

Consider also a collection of points $\{s_1, s_2, \dots, s_J\}$, each $s_j \in \mathbb{R}$, and assume $|s_j - s_{j+1}| \geq \epsilon$ for each j . Define the micro-domains Ω_j^{mic} to be the domains bounded by the curves $x_1 = s_j$ on the left, $x_1 = s_j + \epsilon$ on the right, $x_2 = \gamma > 0$ above, and $\{(x_1, x_2) | x_2 = \zeta^\epsilon(x_1) - \epsilon H\}$ below. The lower curve is simply the portion of Γ^ϵ from $x_1 = s_j$ to $s_j + \epsilon$. Denote this portion of the micro-domains $\partial\Omega_{j, \text{noslip}}^{\text{mic}}$, as this is where the physical wall is located. Denote the remaining portion of the boundary $\partial\Omega_{j, \text{D}}^{\text{mic}} = \partial\Omega_j^{\text{mic}} \setminus \partial\Omega_{j, \text{noslip}}^{\text{mic}}$. Lastly, take γ to be $\mathcal{O}(\epsilon)$. See Figure 3 for an example of such a configuration.

Remark 4.1. In order for the micro-domain problems defined below to be well-posed, the corners of the Ω_j^{mic} domains should be mollified; such technical details are not considered here.

4.1. Multiscale flow model. The purpose of the multiscale model is to efficiently produce an approximation U to the true, oscillatory flow u^ϵ by enforcing U satisfy a wall law of the form from the homogenization theory

$$(4.2) \quad U = \alpha \frac{\partial U_1}{\partial x_2} e_1$$

on Γ , the boundary of the smooth domain Ω^{mac} . The missing data necessary for the model to be complete is the coefficient α in the wall law. The strategy utilized in [4] consists of simply precomputing the solution χ to a (truncated) cell problem and then taking its average $\bar{\chi}$. This constant (plus some amount $\delta \geq \epsilon H$, in light of Theorem 3.2) is then taken to be the missing data α . The precomputing step is possible because the cell problem depends only on the geometry of the roughness.

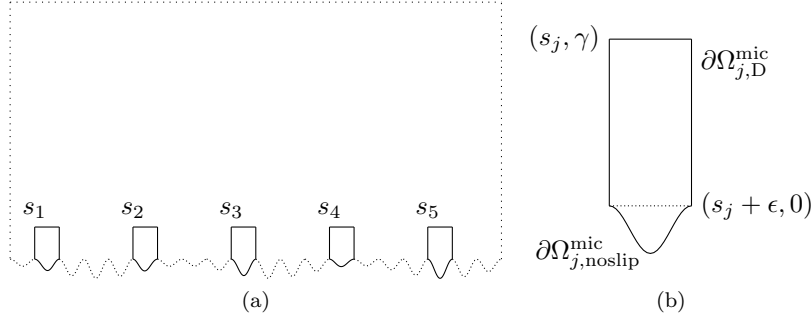


FIG. 3. (a) Example domain Ω^ϵ (.....) containing several Ω_j^{mic} (—). (b) One instance of a micro domain Ω_j^{mic} .

In contrast, the model defined below to estimate α involves coupling a Navier-Stokes system posed in the macroscopic domain Ω^{mac} to J separate Navier-Stokes systems posed in microscopic domains Ω_j^{mic} , $1 \leq j \leq J$. Similar to the cell problem from the homogenization theory, the microscopic systems account for the geometry of the rough surface. They are additionally constrained however to match the averaged local flow values of the macroscopic system, which allows for a more accurate representation of the effect of surface roughness on the macroscopic flow. Furthermore, the inclusion of the nonlinear term allows for convective effects not captured by the cell problem's linear Stokes system. In each Ω_j^{mic} , the ratio of the average flow and the average flow gradient (the shear) is computed. These values are interpolated, and the resulting function is then used for the slip amount α in (4.2). The coupled system is thus designed to reproduce the effective boundary condition from the homogenization theory whenever it is applicable, but also to perform favorably in more general situations to which the theory does not apply.

Define first the macro and microscopic systems, as well as a projection, smoothing, and interpolation operator.

DEFINITION 4.2. Let $M(U, P, \alpha)$ define the following PDE system parameterized by the slip amount α and posed in Ω^{mac} :

$$(4.3) \quad \begin{aligned} -\nu \Delta U + U \nabla U + \nabla P - f &= 0, & \text{in } \Omega^{\text{mac}} \\ \nabla \cdot U &= 0, & \text{in } \Omega^{\text{mac}} \\ U - \alpha \frac{\partial U_1}{\partial x_2} e_1 &= 0, & \text{on } \Gamma \\ U &= 0, & \text{on } \partial \Omega^{\text{mac}} \setminus \Gamma \end{aligned}$$

Note that in general α can vary along Γ so that $\alpha = \alpha(x_1)$.

DEFINITION 4.3. Let $m_j(u^j, p^j, \Upsilon_j)$ define the PDE system posed in Ω_j^{mic} and parameterized by the Dirichlet boundary condition $\Upsilon_j : \partial \Omega_{j,D}^{\text{mic}} \rightarrow \mathbb{R}^2$:

$$(4.4) \quad \begin{aligned} -\nu \Delta u^j + u^j \nabla u^j + \nabla p^j - f &= 0, & \text{in } \Omega_j^{\text{mic}} \\ \nabla \cdot u^j &= 0, & \text{in } \Omega_j^{\text{mic}} \\ u^j &= \Upsilon_j, & \text{on } \partial \Omega_{j,D}^{\text{mic}} \\ u^j &= 0 & \text{on } \partial \Omega_{j,\text{noslip}}^{\text{mic}} \end{aligned}$$

Note that for well-posedness, Υ_j must satisfy

$$(4.5) \quad \int_{\partial\Omega_{j,D}^{\text{mic}}} \Upsilon_j \cdot n \, ds = 0.$$

Furthermore, let $\{s_n\}_{n=1}^{\infty} \in \partial\Omega_{j,D}^{\text{mic}}$ be some convergent sequence whose limiting point $\sigma = (s_j, 0)$ or $\sigma = (s_j + \epsilon, 0)$. Then Υ_j should also satisfy

$$(4.6) \quad \lim_{n \rightarrow \infty} \Upsilon_j(s_n) = 0$$

for continuity with the no slip condition posed along $\partial\Omega_{j,\text{noslip}}^{\text{mic}}$.

DEFINITION 4.4. *For a sufficiently regular class of functions \mathcal{S} , let*

$$(4.7) \quad \pi_j : \mathcal{S}(\Omega^{\text{mac}}) \rightarrow \mathcal{S}(\partial\Omega_{j,D}^{\text{mic}})$$

Then for some $f \in \mathcal{S}(\Omega^{\text{mac}})$, let $\pi_j(f)$ satisfy the properties (4.5) and (4.6).

This projection operator is the mechanism by which the micro-domain is constrained by the macroscopic solution U . Note that simply taking the trace of U along $\partial\Omega_{j,D}^{\text{mic}}$ is not appropriate, since even though the conservation of mass property (4.5) holds, the constraint (4.6) will not. π_j of course is not uniquely defined by these constraints, however two specific definitions will be proposed below—one for the specific case of periodic roughness and horizontal macro flow, and another for more general settings.

DEFINITION 4.5. *For integrable $u : \mathbb{R}^2 \rightarrow \mathbb{R}$ and $y \in \mathbb{R}$, define the operator*

$$(4.8) \quad \langle u \rangle(x, y) := \int_x^{x+\epsilon} u(s, y) \, ds$$

which integrates u in the horizontal direction along a small, ϵ -sized strip $[x, x + \epsilon]$ at fixed height y .

DEFINITION 4.6. *For collection of J points $\{(s_1, \alpha_1), \dots, (s_J, \alpha_J)\}$, $(s_j, \alpha_j) \in \mathbb{R}^2$, define*

$$(4.9) \quad \mathcal{I}((s_1, \alpha_1), \dots, (s_J, \alpha_J)) : \mathbb{R}^{2 \times J} \rightarrow C(\mathbb{R})$$

to be a piecewise continuous polynomial interpolant based on the given points.

Using the above definitions, the multiscale flow model is formally defined as follows; given a collection of points $\{s_j\}_{j=1}^J$ along the rough domain Γ^ϵ , find (U, P) and $((u^1, p^1), \dots, (u^J, p^J))$ satisfying the coupled system of equations:

$$(4.10) \quad M(U, P, \alpha) = 0$$

$$(4.11) \quad m_j(u^j, p^j, \Upsilon_j) = 0, \quad 1 \leq j \leq J$$

$$(4.12) \quad \Upsilon_j = \pi_j(U), \quad 1 \leq j \leq J$$

$$(4.13) \quad \alpha_j = \langle u_1^j \rangle(s_j, 0) / \langle \partial u_1^j / \partial x_2 \rangle(s_j, 0), \quad 1 \leq j \leq J$$

$$(4.14) \quad \alpha = \mathcal{I}((s_1, \alpha_1), \dots, (s_J, \alpha_J)).$$

A key feature of the method clearly is the specification of the locations $\{s_1, \dots, s_J\}$ of the micro-domains Ω_j^{mic} . A general strategy is to choose to simulate at a location s_j where either the roughness varies nontrivially or the macroscopic flow is qualitatively different, or both. For Poiseuille type channel flow with periodic roughness, for

instance, only one micro-domain covering a single periodic roughness element is necessary. In more realistic applications for which the surface roughness is nonperiodic and additionally varies over macroscopic length scales, the micro-domain should be chosen large enough to cover a few of the estimated correlation lengths, or approximate periods. They should also be placed frequently enough along Γ^ϵ to capture its large-scale, macroscopic variations. The numerical examples in [section 5](#) are chosen to approximate such situations.

4.2. Algorithm for the coupled system. In practice, the coupled, stationary system (4.10)-(4.14) is solved iteratively. Let $\tau > 0$ be some fixed tolerance, and let the subscript (k) denote the value of a quantity at the k^{th} iteration of the procedure.

Starting from an initial guess $\alpha_{(0)} = 0$ (i. e. no slip along Γ), the macro-problem is solved for $U_{(0)}$. The J micro-problems are then solved, and a new estimate for the slip amount $\alpha_{(1)}$ is obtained. If the relative difference between the new and old slip amount is smaller than τ , the iteration is terminated, and one final solve for the macroscopic solution U is required. Otherwise, the procedure is repeated. [Algorithm 4.1](#) details the method more precisely.

Algorithm 4.1 Compute macroscopic approximation (U, P) to (u^ϵ, p^ϵ)

```

1: Inputs:  $\{s_1, \dots, s_J\}, \tau$ 
2:  $\alpha_{(0)} \leftarrow 0$ 
3: solve  $M(U_{(0)}, P_{(0)}, \alpha_{(0)}) = 0$ 
4: for  $k = 1, 2, 3, \dots$  do
5:   for  $j = 1, \dots, J$  do
6:      $\Upsilon_j \leftarrow \pi_j(U_{(k-1)})$ 
7:     solve  $m_j(u_{(k)}^j, p_{(k)}^j, \Upsilon_j) = 0$ 
8:
9:      $\alpha_j \leftarrow \langle u_{1,(k)}^j \rangle(s_j, 0) / \langle \partial u_{1,(k)}^j / \partial x_2 \rangle(s_j, 0)$ 
10:   end for
11:    $\alpha_{(k)} \leftarrow \mathcal{I}((s_1, \alpha_1), \dots, (s_J, \alpha_J))$ 
12:   if  $\|\alpha_{(k)} - \alpha_{(k-1)}\|_\infty < \tau$  then
13:     terminate loop
14:   else
15:     solve  $M(U_{(k)}, P_{(k)}, \alpha_{(k)}) = 0$ 
16:      $U_{(k-1)} \leftarrow U_{(k)}$ 
17:   end if
18: end for
19: solve  $M(U_{(k)}, P_{(k)}, \alpha_{(k)}) = 0$ 
20: Return:  $(U_{(k)}, P_{(k)})$ 

```

Remark 4.7. Since the microscopic systems $m_j(u^j, p^j, \Upsilon_j)$ are independent of one another, they are trivially parallelizable.

Remark 4.8. If the relative error tolerance $\tau = \epsilon^2$ is prescribed, [Algorithm 4.1](#) is observed in practice to terminate after only one iteration; that is, the condition $|\alpha_{(1)} - \alpha_{(2)}| < \epsilon^2$ always holds. This statement is justified in [subsection 4.4](#) below and is observed in all cases reported in [section 5](#). Hence, the outermost for-loop in [Algorithm 4.1](#) can actually be terminated at line 11 for $k = 1$.

4.3. Boundary conditions for the microscopic systems. Given some macroscopic flow U , each of the microscopic problems depends on the boundary condition from the projection operator

$$(4.15) \quad u^j = \Upsilon_j = \pi_j(U), \quad \text{on } \partial\Omega_{j,D}^{\text{mic}}.$$

In the case when U is horizontal, i. e. the vertical component of the velocity vector is zero (or at least asymptotically small compared with the horizontal component), then the boundary condition can be simplified to a “free stream” condition along the upper computational boundary $x_2 = \gamma$

$$(4.16) \quad u^j = \langle U \rangle (s_j, \gamma) e_1$$

and periodic boundary conditions at $x_1 = s_j$ and $x_1 = s_j + \epsilon$. In this case π_j maps to functions on $\partial\Omega_{j,D}^{\text{mic}} = \{(x_1, x_2) | s_j \leq x_1 < s_j + \epsilon, x_2 = \gamma\}$.

In more general situations in which the macroscopic flow has nontrivial dependence on x_1 and/or a nontrivial vertical component, a more general approach is needed. We propose to prescribe quadratic Dirichlet conditions for both the horizontal and vertical components of the velocity along each of the three faces of $\partial\Omega_{j,D}^{\text{mic}}$ (those that intersect $x_1 = s_j$, $x_1 = s_j + \epsilon$ and $x_2 = \gamma$). Let

$$(4.17) \quad \Gamma_1^{\text{mic}} = \{(x_1, x_2) | 0 \leq x_2 \leq \gamma, x_1 = s_j\}$$

$$(4.18) \quad \Gamma_2^{\text{mic}} = \{(x_1, x_2) | s_j \leq x_1 \leq s_j + \epsilon, x_2 = \gamma\}$$

$$(4.19) \quad \Gamma_3^{\text{mic}} = \{(x_1, x_2) | 0 \leq x_2 \leq \gamma, x_1 = s_j + \epsilon\}$$

be the left, upper, and right computational boundaries of the micro-domain (the dependence of each Γ_k^{mic} on j is implied). Then there are two quadratic profiles for each boundary, each with three coefficients to be determined, and hence 18 total constraints are needed. Let u_k and v_k be the quadratic profile for the horizontal and vertical component of the flow at Γ_k^{mic} , $k = 1, 2, 3$. The no slip requirement (4.6) gives four constraints

$$(4.20) \quad 0 = u_1(s_j, 0) = v_1(s_j, 0) = u_3(s_j + \epsilon, 0) = v_3(s_j + \epsilon, 0).$$

Additionally, enforce that the mass flux across each Γ_k^{mic} is the same as the macroscopic mass flux

$$(4.21) \quad \int_{\Gamma_1^{\text{mic}}} u_1 ds = \int_{\Gamma_1^{\text{mic}}} U \cdot n ds$$

$$(4.22) \quad \int_{\Gamma_2^{\text{mic}}} v_2 ds = \int_{\Gamma_2^{\text{mic}}} U \cdot n ds$$

$$(4.23) \quad \int_{\Gamma_3^{\text{mic}}} u_3 ds = \int_{\Gamma_3^{\text{mic}}} U \cdot n ds.$$

Since U is divergence free, these imply conservation of mass along the micro-domain boundaries

$$(4.24) \quad \int_{\Gamma_1^{\text{mic}}} u_1 ds + \int_{\Gamma_2^{\text{mic}}} v_2 ds + \int_{\Gamma_3^{\text{mic}}} u_3 ds = 0,$$

hence satisfying requirement (4.5). This gives three more conditions. In order to completely specify the quadratic profiles, one more condition each is needed for u_1

and u_3 , two more conditions are needed for v_1 , v_2 , and v_3 , and three conditions are needed for u_2 . For continuity, enforce

$$(4.25) \quad u_1(s_j, \gamma) = u_2(s_j, \gamma) = U(s_j, \gamma) \cdot e_1$$

$$(4.26) \quad v_1(s_j, \gamma) = v_2(s_j, \gamma) = U(s_j, \gamma) \cdot e_2$$

$$(4.27) \quad u_2(s_j + \epsilon, \gamma) = u_3(s_j + \epsilon, \gamma) = U(s_j + \epsilon, \gamma) \cdot e_1$$

$$(4.28) \quad v_2(s_j + \epsilon, \gamma) = v_3(s_j + \epsilon, \gamma) = U(s_j + \epsilon, \gamma) \cdot e_2,$$

which leaves one more condition each for v_1 , u_2 , and v_3 . Adding one more interpolation point for each

$$(4.29) \quad v_1(s_j, \gamma/2) = U(s_j, \gamma/2) \cdot e_2$$

$$(4.30) \quad u_2(s_j + \epsilon/2, \gamma) = U(s_j + \epsilon/2, \gamma) \cdot e_1$$

$$(4.31) \quad v_3(s_j + \epsilon, \gamma/2) = U(s_j + \epsilon, \gamma) \cdot e_2.$$

ensures the Dirichlet conditions are thus uniquely determined along each Γ_k^{mic} , which defines the projection operator π_j . The method is tested in [section 5](#).

4.4. Convergence theory for domains with periodic roughness. Next we show that if one assumes (i) periodic roughness in the macroscopic domain (i. e. $\beta = 1$) and (ii) the solution u to the microscopic problem (4.4) can be expanded in the form

$$(4.32) \quad u = \bar{u} + u^{\text{loc}} + \mathcal{O}(\epsilon^2),$$

as in [subsection 3.2](#), then the HMM algorithm reproduces the slip constant $\epsilon(\bar{\chi} + H)$ from [4] up to an asymptotic error of $\mathcal{O}(\epsilon^{3/2})$. Here \bar{u} is assumed to satisfy the effective boundary condition

$$(4.33) \quad \bar{u} = \epsilon(\bar{\chi} + H) \frac{\partial \bar{u}_1}{\partial x_2} e_1$$

on Γ , and

$$(4.34) \quad u^{\text{loc}} = \epsilon \frac{\partial \bar{u}_1}{\partial x_2}(x_1, 0) (\chi(x/\epsilon) - \bar{\chi})$$

in Ω^{mic} , where $\chi - \bar{\chi}$ solves the cell problem (3.22).

If only one micro-simulation is performed at some $x_1 = z$, then by definition the slip amount is given by (4.13):

$$(4.35) \quad \alpha = \frac{\langle \bar{u}_1 \rangle(z, 0) + \langle u_1^{\text{loc}} \rangle(z, 0) + \mathcal{O}(\epsilon^3)}{\langle \partial \bar{u}_1 / \partial x_2 \rangle(z, 0) + \langle \partial u_1^{\text{loc}} / \partial x_2 \rangle(z, 0) + \mathcal{O}(\epsilon^3)},$$

where $\langle \mathcal{O}(\epsilon^2) \rangle = \mathcal{O}(\epsilon^3)$ is used.

Assume for now (it will be shown below) that, up to an error of $\mathcal{O}(\epsilon^{5/2})$ (respectively $\mathcal{O}(\epsilon^{3/2})$), the integral of u_1^{loc} (resp. $\partial u_1^{\text{loc}} / \partial x_2$) vanishes. Then the above expression reduces to

$$(4.36) \quad \alpha = \frac{\langle \bar{u}_1 \rangle(z, 0) + \mathcal{O}(\epsilon^{5/2})}{\langle \partial \bar{u}_1 / \partial x_2 \rangle(z, 0) + \mathcal{O}(\epsilon^{3/2})}.$$

The integrand in the term $\langle \bar{u}_1 \rangle (z, 0)$ in the numerator

$$(4.37) \quad \langle \bar{u}_1 \rangle (z, 0) = \int_z^{z+\epsilon} \bar{u}_1(s, 0) ds$$

can be Taylor expanded about the point z

$$(4.38) \quad \bar{u}_1(s, 0) = \bar{u}_1(z, 0) + \frac{\partial \bar{u}_1}{\partial x_1}(z, 0)(s - z) + \frac{\partial^2 \bar{u}_1}{\partial x_1^2}(\xi(s), 0)(s - z)^2/2,$$

which yields

$$(4.39) \quad \langle u_1^{m,1} \rangle (z, 0) = \epsilon \bar{u}_1(z, 0) + \mathcal{O}(\epsilon^2),$$

after insertion into the integration operator $\langle \cdot \rangle$. A similar computation for the $\langle \partial \bar{u}_1 / \partial x_2 \rangle (z, 0)$ term in the denominator produces

$$(4.40) \quad \left\langle \frac{\partial \bar{u}_1}{\partial x_2} \right\rangle (z, 0) = \epsilon \frac{\partial \bar{u}_1}{\partial x_2}(z, 0) + \mathcal{O}(\epsilon^{3/2}).$$

where the Prandtl boundary layer scale assumption $\partial \bar{u}_1 / \partial x_2(z, 0) = \mathcal{O}(\epsilon^{-1/2})$ is made, as in [subsection 3.2](#). As a result,

$$(4.41) \quad \begin{aligned} \alpha &= \frac{\epsilon \bar{u}_1(z, 0) + \mathcal{O}(\epsilon^2)}{\epsilon \frac{\partial \bar{u}_1}{\partial x_2}(z, 0) + \mathcal{O}(\epsilon^{3/2})} = \frac{\epsilon(\bar{\chi} + H) + \mathcal{O}(\epsilon^{3/2})}{1 + \mathcal{O}(\epsilon)} \\ &= \epsilon(\bar{\chi} + H) + \mathcal{O}(\epsilon^{3/2}) \end{aligned}$$

where the final equality results from

$$(4.42) \quad \frac{1}{1+x} = 1 + \mathcal{O}(x), \quad |x| < 1,$$

which gives the desired result. It remains to show that

$$(4.43) \quad \begin{aligned} |\langle u_1^{\text{loc}} \rangle (z, 0)| &\leq C_1 \epsilon^{5/2} \\ |\langle \partial u_1^{\text{loc}} / \partial x_2 \rangle (z, 0)| &\leq C_2 \epsilon^{3/2}. \end{aligned}$$

First consider $|\langle u_1^{\text{loc}} \rangle| = \left| \left\langle \epsilon \frac{\partial \bar{u}_1}{\partial x_2}(s, 0) (\chi_1(x/\epsilon) - \bar{\chi}) \right\rangle \right|$. By definition,

$$(4.44) \quad \bar{\chi} = \hat{\chi}_1(k=0, y_2) = \int_0^1 \chi_1(y_1, y_2) dy_1, \quad \forall y_2 \geq 0,$$

i.e. $\bar{\chi}$ is the zeroth Fourier mode of χ and is independent of y_2 . Observe that if $\partial \bar{u}_1 / \partial x_2(s, 0)$ were constant in s , then $\langle u_1^{\text{loc}} \rangle (z, 0) = 0$ would result. Instead, a Taylor expansion of $\partial \bar{u}_1 / \partial x_2(s, 0)$ about the point z gives

$$(4.45)$$

$$(4.46) \quad \left| \left\langle \epsilon \frac{\partial \bar{u}_1}{\partial x_2}(s, 0) (\chi_1(s/\epsilon) - \bar{\chi}) \right\rangle (z, 0) \right| \leq \epsilon \left| \frac{\partial \bar{u}_1}{\partial x_2}(z, 0) \right| \cdot \overbrace{|\langle \chi_1 - \bar{\chi} \rangle (z, 0)|}^{=0}$$

$$(4.47) \quad + \epsilon \left| \frac{\partial^2 \bar{u}_1}{\partial x_2 \partial x_1}(z, 0) \right| \cdot |\langle (s - z) (\chi_1 - \bar{\chi}) \rangle (z, 0)|$$

$$(4.47) \quad + \epsilon \left| \left\langle \frac{\partial^3 \bar{u}_1}{\partial x_2 \partial x_1^2}(\xi(s), 0) \frac{(s - z)^2}{2} (\chi_1 - \bar{\chi}) \right\rangle (z, 0) \right|.$$

Further bounding the above

$$\begin{aligned}
(4.46) &\leq \epsilon \left| \frac{\partial^2 \bar{u}_1}{\partial x_2 \partial x_1}(z, 0) \right| \int_z^{z+\epsilon} |(s-z)| |\chi_1(s/\epsilon, 0) - \bar{\chi}| ds \\
(4.48) &\leq \frac{\epsilon^3}{2} \left| \frac{\partial^2 \bar{u}_1}{\partial x_2 \partial x_1}(z, 0) \right| \cdot \sup_{y_1 \in [0,1]} |\chi_1(y_1, 0) - \bar{\chi}| = \mathcal{O}(\epsilon^{5/2}), \\
(4.47) &\leq \frac{\epsilon^4}{6} \sup_{s \in [z, z+\epsilon]} \left| \frac{\partial^3 \bar{u}_1}{\partial x_2 \partial x_1^2}(\xi(s), 0) (\chi_1(s/\epsilon, 0) - \bar{\chi}) \right| = \mathcal{O}(\epsilon^{7/2}).
\end{aligned}$$

shows that $\left| \langle u_1^{\text{loc}} \rangle(z, 0) \right| \leq C_1 \epsilon^{5/2}$. To bound the integral of $\partial u_1^{\text{loc}} / \partial x_2$, first note that again, if $\partial \bar{u}_1 / \partial x_2(s, 0)$ were constant in s , then

$$\begin{aligned}
(4.49) \quad \left\langle \frac{\partial u_1^{\text{loc}}}{\partial x_2} \right\rangle(z, 0) &= \epsilon \frac{\partial \bar{u}_1}{\partial x_2} \left\langle \frac{\partial}{\partial x_2} (\chi_1 - \bar{\chi}) \right\rangle(z, 0) \\
(4.50) &= \frac{\partial \bar{u}_1}{\partial x_2} \int_z^{z+\epsilon} \frac{\partial \chi_1}{\partial y_2}(s/\epsilon, 0) ds \\
(4.51) &= \frac{\partial \bar{u}_1}{\partial x_2} \frac{d}{dy_2} \int_z^{z+\epsilon} \chi_1(s/\epsilon, 0) ds \\
(4.52) &= 0
\end{aligned}$$

by the Leibniz rule. Instead, expand $\partial \bar{u}_1 / \partial x_2$ in a Taylor series to get

$$\begin{aligned}
(4.53) \quad \left| \left\langle \epsilon \frac{\partial \bar{u}_1}{\partial x_2}(s, 0) \frac{\partial \chi_1}{\partial x_2} \right\rangle(z, 0) \right| &\leq \epsilon \left| \frac{\partial \bar{u}_1}{\partial x_2}(z, 0) \right| \cdot \overbrace{\left| \left\langle \frac{\partial \chi_1}{\partial x_2} \right\rangle(z, 0) \right|}^{=0} \\
(4.54) &+ \epsilon \left| \frac{\partial^2 \bar{u}_1}{\partial x_2 \partial x_1}(z, 0) \right| \cdot \left| \left\langle (s-z) \frac{\partial \chi_1}{\partial x_2} \right\rangle(z, 0) \right| \\
(4.55) &+ \epsilon \left| \left\langle \frac{\partial^3 \bar{u}_1}{\partial x_2 \partial x_1^2}(\xi(s), 0) \frac{(s-z)^2}{2} \frac{\partial \chi_1}{\partial x_2} \right\rangle(z, 0) \right|,
\end{aligned}$$

which can be bounded as follows

$$\begin{aligned}
(4.56) \quad (4.54) &\leq \frac{\epsilon^2}{2} \left| \frac{\partial^2 \bar{u}_1}{\partial x_2 \partial x_1}(z, 0) \right| \cdot \sup_{y_1 \in [0,1]} \left| \frac{\partial \chi_1}{\partial y_2}(y_1, 0) \right| = \mathcal{O}(\epsilon^{3/2}) \\
(4.57) \quad (4.55) &\leq \frac{\epsilon^3}{6} \sup_{s \in [z, z+\epsilon]} \left| \frac{\partial^3 \bar{u}_1}{\partial x_2 \partial x_1^2}(\xi(s), 0) \right| \cdot \sup_{y_1 \in [0,1]} \left| \frac{\partial \chi_1}{\partial y_2}(y_1, 0) \right| = \mathcal{O}(\epsilon^{5/2})
\end{aligned}$$

as desired.

In summary, we have shown that for domains with periodic roughness, the slip constant α defined by the HMM scheme equals the slip constant $\epsilon(\bar{\chi} + H)$ from [4], plus a perturbation of $\mathcal{O}(\epsilon^{3/2})$. The result relies on the validity of the asymptotic analysis of [4] in the microscopic domain, and in particular assumes that the mean flow is smooth.

5. Numerical results. We now present numerical tests of the HMM scheme both in situations where the periodic homogenization theory is applicable and where it is not. All computations are performed using the open source finite element package FEniCS [30, 31], and all meshes are generated using Gmsh [21]. In the first four cases

considered, $\epsilon = 0.025$ and $|\Omega^{\text{mac}}| = \mathcal{O}(1)$, and $\nu = 1$. Strictly speaking, this set of parameters is not in the asymptotic regime analyzed in [section 3](#); however, the assumption [\(3.3\)](#) certainly holds. Different values are prescribed for the final example of a backwards facing step and are detailed below. In all cases, the parameter defining the upper boundary of the microscopic domain $\gamma = 4\epsilon$.

All discretizations are performed with the Taylor-Hood elements, i.e. P_2 and P_1 basis functions for the velocity and pressure fields, respectively [\[25, 29\]](#), and the resulting discrete nonlinear system is solved with Newton’s method, using the solution to the corresponding Stokes problem as the initial guess.

The direct numerical simulation (DNS) of the full problem [\(3.2\)](#) is computed with a large number of elements and is compared with (i) the 1st order approximation satisfying the no slip condition along Γ and (ii) the HMM approximation satisfying the coupled system [\(4.10\)](#)-[\(4.13\)](#), both of which are computed on the same mesh. The coupled HMM system is solved iteratively, using [Algorithm 4.1](#). The tolerance τ for the relative error between successive slip amounts α is set to be $\tau = \epsilon^2$.

In all cases, the HMM solution is clear improvement over the first order, no slip approximation; it captures the average effect of roughness on the flow. Of particular note is the final example of a backwards facing step, for which the HMM solution correctly captures the effect of the roughness on the size of the recirculation bubble.

5.1. Flow in a channel with periodic roughness. First consider a channel domain with periodic roughness, as in [Figure 4a](#). The macroscopic domain is simply $\Omega^{\text{mac}} = [0, 1]^2$, and the roughness is parameterized by the function $\varphi^\epsilon(x_1) = \epsilon/2(\cos(2\pi x_1/\epsilon) - 1)$. The no slip condition is applied at the upper boundary $x_2 = 1$, and periodic boundary conditions are applied on the left/right boundaries. A constant pressure gradient $-\nabla p = (1 \ 0)^T$ drives the flow from left to right. Ω^ϵ is discretized with 50554 cells, while the discretization of Ω^{mac} and Ω^{mic} contain only 3200 and 927 cells, totaling $6.3\% + 1.8\% = 8.1\%$ the amount of rough domain cells.

In the setting just described, the macroscopic solution U is one dimensional. Only the horizontal component of the flow is nonzero, and it only depends on the wall-normal variable x_2 . In this case, only one micro-domain is needed, and periodic boundary conditions can be prescribed along the left/right computational boundaries of the micro-domain ($x_1 = s$ and $x_1 = s + \epsilon$) for simplicity, as discussed in [subsection 4.3](#). The free stream condition [\(4.16\)](#) is then applied along the upper computational boundary $x_2 = 4\epsilon$.

[Figure 5](#) and [Figure 6](#) plot u_1 and $\partial u_1/\partial x_2$, respectively, as functions of x_1 for various values of x_2 near the wall. Also computed was an HMM solution using the more general strategy for the projection operator π_j defined by the constraints [\(4.20\)](#)-[\(4.31\)](#) (not pictured). The resulting slip amount differed from the one computed with periodic boundary conditions in the micro domain only by 0.9%. It is interesting to note, however, that the micro-domain flow u_1 along the line $x_2 = 0$ over which the average is taken has a lower value in the Dirichlet case than in the periodic case. Accordingly, the shear $\partial u_1/\partial x_2$ is lower as well.

5.2. Nonsquare domain with periodic roughness. Next, consider a non-square macroscopic domain with periodic, “sawtooth” roughness as shown in [Figure 4b](#). Let $h(x_1) := 0.5 - 0.125\sin(2\pi x_1)$. Then

$$(5.1) \quad \Omega^{\text{mac}} = \{(x_1, x_2) | 0 \leq x_1 \leq 1, 0 \leq x_2 \leq h(x_1)\}.$$

The roughness is parameterized by the periodic function $\varphi^\epsilon(x_1) = -3\epsilon/4(x_1/\epsilon - [x_1/\epsilon])$. The no slip condition is applied on the domain’s upper, curved boundary,

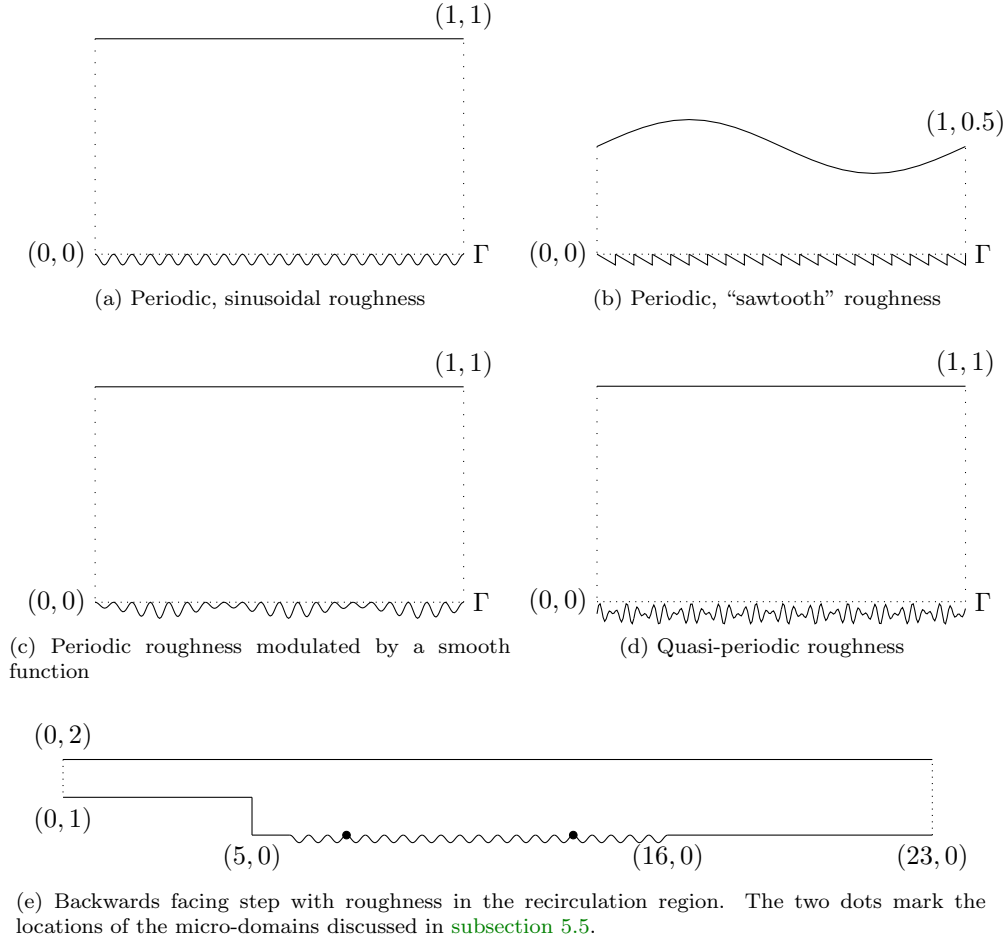


FIG. 4. Sketches of the rough domains used to test the numerical method.

and periodic boundary conditions are applied on the left/right boundaries. A constant body force $f = (1 \ 0)^T$ drives the flow from left to right. Ω^ϵ is discretized with 41898 cells, while Ω^{mac} is discretized with only 1854 cells and each of the five discretized Ω^{mic} domains below contain 903 cells, totaling $4.4\% + 11.0\% = 15.4\%$ the amount of rough domain cells.

To compute the HMM approximations, we use [Algorithm 4.1](#) and set

$$(5.2) \quad \{s_1, s_2, s_3, s_4, s_5\} = \{0, 0.25, 0.5, 0.75, 1\}$$

chosen to capture influence of the macroscopic curvature of Ω^{mac} . The percent difference between the largest and smallest resulting values of slip amounts is a negligible 0.3%, indicating that simply performing one micro-solve at a single s_j is sufficient in this case.

In contrast to the previous example, the macroscopic flow U is not one dimensional, i. e. both U_2 and $\partial U_1 / \partial x_1$ are nonzero, as can be seen from the DNS curve in [Figure 7](#) and [Figure 8](#). However, since at $x_2 = 4\epsilon$ the horizontal component of the flow is approximately one order of magnitude larger than the vertical component for a given x_1 , it is reasonable to attempt to approximate the vertical component as being

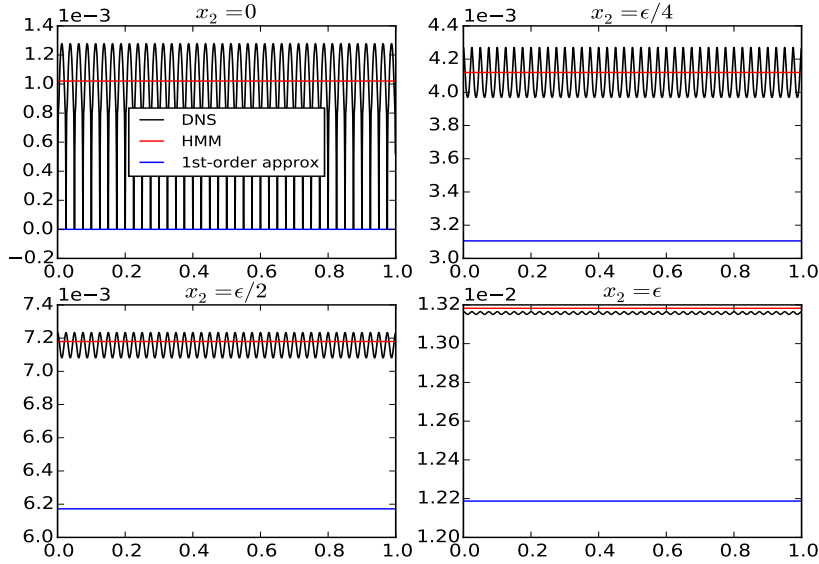


FIG. 5. Horizontal component of the flow u_1 versus x_1 plotted at various heights x_2 for the domain shown in Figure 4a.

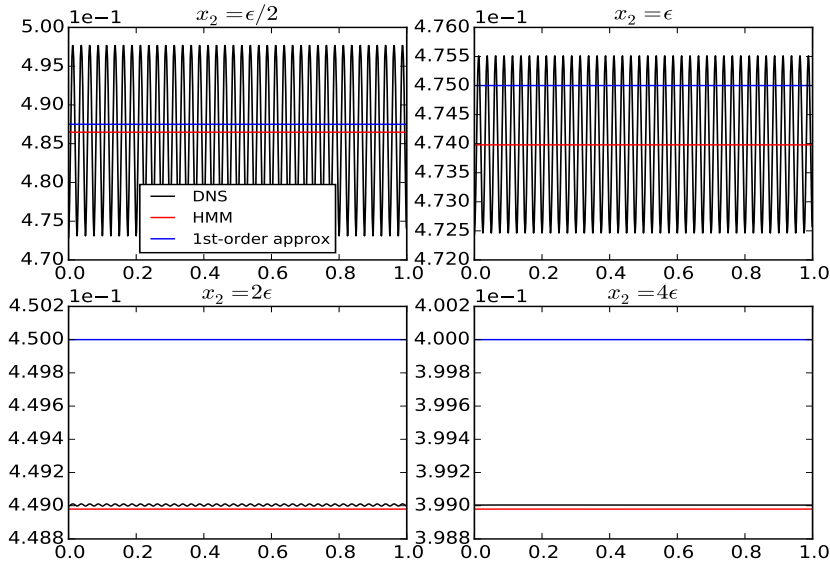


FIG. 6. Shear $\partial u_1 / \partial x_2$ versus x_1 plotted at various heights x_2 for the domain shown in Figure 4a.

zero and compute with periodic boundary conditions and the free-stream condition (4.16).

Similar to the previous numerical example in [subsection 5.1](#) a difference of about one percent is observed between the slip amount computed this way and the slip amount using the more general projection $\pi_j(U)$.

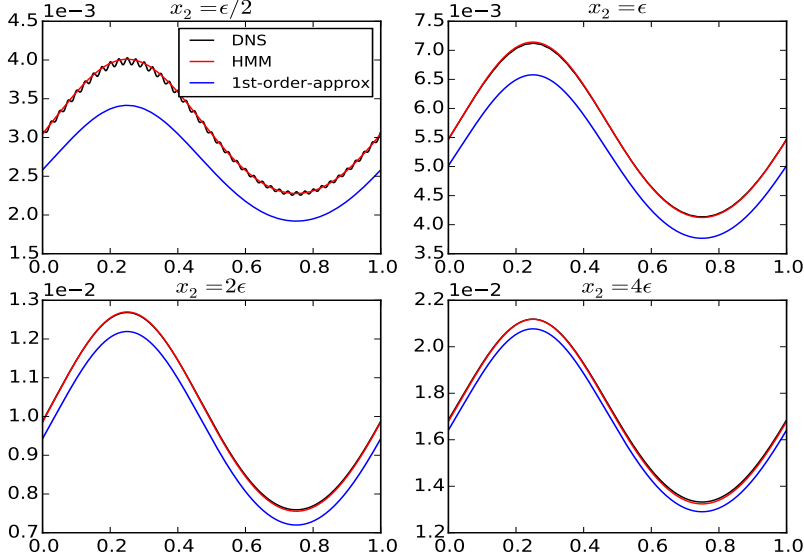


FIG. 7. Horizontal component of the flow u_1 versus x_1 plotted at various heights x_2 for the domain shown in [Figure 4b](#).

The results in [Figure 7](#) and [Figure 9](#) again show u_1 and $\partial u_1 / \partial x_2$ versus x_1 for various values of x_2 .

5.3. Flow in a channel with non-periodic roughness. Consider again $\Omega^{\text{mac}} = [0, 1]^2$, but now let the roughness be parameterized by

$$(5.3) \quad \zeta^\epsilon(x_1) = \beta(x_1)\varphi^\epsilon(x_1)$$

$$(5.4) \quad \beta(x_1) = \sin^2\left(\sqrt{2}2\pi x_1\right) + 0.5$$

$$(5.5) \quad \varphi^\epsilon(x) = \epsilon/2(\cos(2\pi x_1/\epsilon) - 1),$$

so that the periodic roughness is modulated by a smooth function as shown in [Figure 4c](#). The no slip condition is applied at $x_2 = 1$, periodic boundary conditions are enforced at $x_1 = 0$ and $x_1 = 1$, and a uniform pressure gradient $-\nabla p = (1 \ 0)^T$ drives the flow from left to right. Ω^ϵ is discretized with 51210 cells, while Ω^{mac} is discretized with only 3200 cells and the sum of the discrete cells in the 7 separate micro domains below totals 9779, amounting to 6.3% + 12.8% = 19.1% of the rough domain cells.

[Algorithm 4.1](#) is used with

$$(5.6) \quad \{s_1, s_2, s_3, s_4, s_5, s_6, s_7\} = \{0, 0.15, 0.35, 0.525, 0.675, 0.875, 0.975\}$$

chosen to capture the large scale curvature of β . The asymptotic analysis presented in [subsection 3.2](#) suggests it is sufficient to simply compute in a single microscopic domain with roughness parameterized only by φ^ϵ and then multiply the resulting

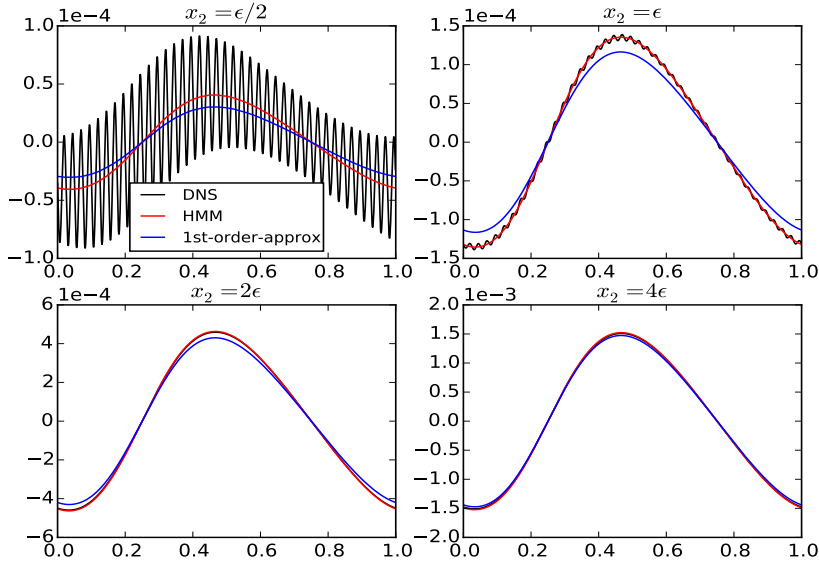


FIG. 8. Vertical component of the flow u_2 versus x_1 plotted at various heights x_2 for the domain shown in Figure 4b.

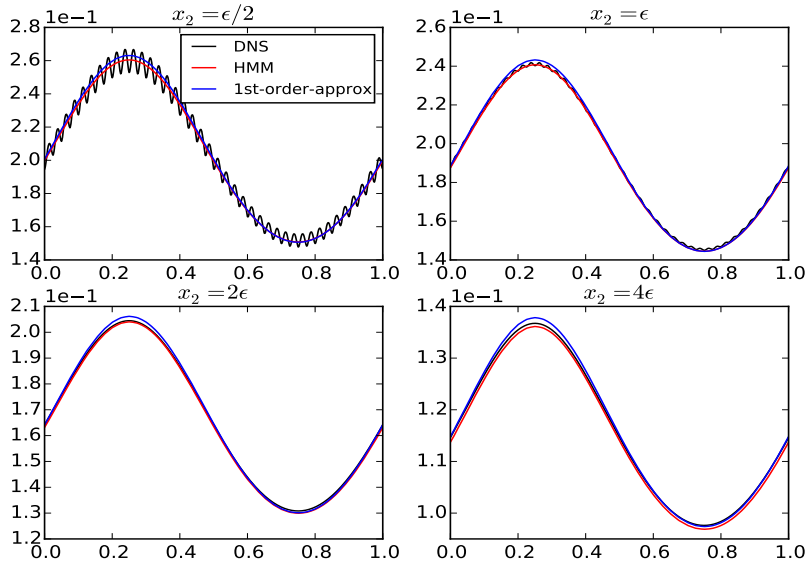


FIG. 9. Shear $\partial u_1 / \partial x_2$ versus x_1 plotted at various heights x_2 for the domain shown in Figure 4b.

slip amount by $\beta(x_1)$ in the effective boundary condition (4.2). However, we chose to apply the general HMM algorithm to mimic the situation in which an analytic

formula for β is not known.

In this case, the percent difference between the largest and smallest slip amounts is a non-negligible 23.4%. [Figure 10](#) and [Figure 11](#) illustrate the success of the HMM method in capturing the horizontal dependence of the slip amount.

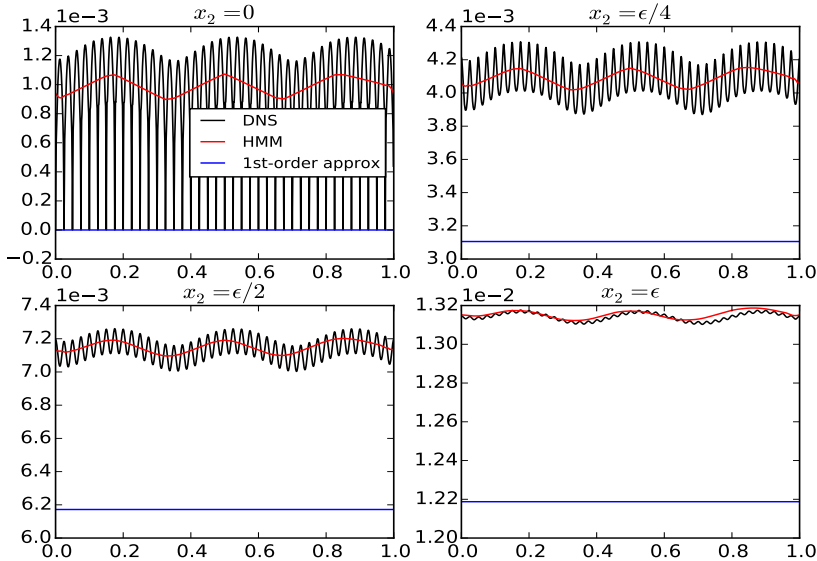


FIG. 10. Horizontal component of the flow u_1 versus x_1 plotted at various heights x_2 for the domain shown in [Figure 4c](#).

5.4. Flow in a channel with quasi-periodic roughness. Consider now a rough boundary parameterized by the quasi-periodic function

$$(5.7) \quad \varphi(x_1/\epsilon) = \epsilon/3 \left(\sin(\sqrt{2} \cdot 2\pi x_1/\epsilon) + \sin(2\pi x_1/\epsilon) - 2.25 \right),$$

like the one displayed in [Figure 4d](#). As in [subsection 5.1](#) and [subsection 5.3](#), $\Omega^{\text{mac}} = [0, 1]^2$, and no slip is applied at $x_2 = 0$. For both Ω^ϵ and Ω^{mac} , periodic boundary conditions are applied at $x_1 = 0$ and $x_1 = 1$. For u^ϵ this is only an approximation, since φ^ϵ is not truly periodic, which explains the spurious boundary layers in the DNS solution near $x_1 = 0$ and $x_1 = 1$, as seen in [Figure 12](#) and [Figure 13](#).

The same problem is encountered in the micro-domain if periodic boundary conditions are prescribed. Instead, we use the Dirichlet boundary conditions defined by the projection operator π_j with constraints (4.20)-(4.31). In this case the no slip condition (4.20) is applied at the more general locations $(s_j, \varphi^\epsilon(s_j))$ and $(s_j + L, \varphi^\epsilon(s_j + L))$, where L is the generalized horizontal length of the micro-domain. In any case it is best to take $L > \epsilon$ in order to capture a few ‘‘correlation lengths’’ of φ^ϵ .

The computations shown in [Figure 12](#) and [Figure 13](#) are performed with one micro domain at $s_1 = 0.481561$ and length $L = 5\epsilon$. Ω^ϵ is discretized with 65568 cells, while Ω^{mac} and Ω^{mic} are discretized with 3280 and 5028 cells, totaling $5\% + 7.7\% = 12.7\%$ the amount of rough domain cells.

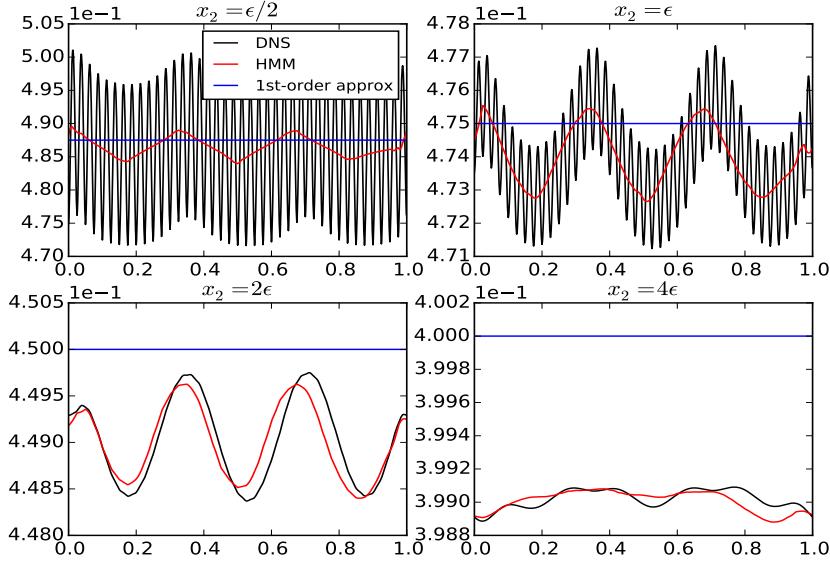


FIG. 11. Shear $\partial u_1/\partial x_2$ versus x_1 plotted at various heights x_2 for the domain shown in Figure 4c.

We note also that if one still wants to use periodic boundary conditions, another option is to further increase the horizontal domain length L and then replace the averaging operator Definition 4.5 with

$$(5.8) \quad \langle u \rangle (x, y) = \int_x^{x+L} K(s)u(s, y) ds$$

where K is smooth function that has compact support, integrates to unity, and satisfies some vanishing moment conditions. Such kernels are well known in the numerical homogenization community [18, 22, 7] and probably would be useful in realistic applications beyond the academic test cases presented here.

5.5. Flow over a backwards facing step. Consider now flow over a backwards facing step with periodic roughness after the step, as in Figure 4e. The roughness is parameterized by the function

$$(5.9) \quad \varphi^\epsilon(x) = \epsilon/2 (\cos(2\pi x_1/\lambda) - 1),$$

similar to subsection 5.1 but with a larger wavelength $\lambda = 2.5\epsilon$. We are primarily interested in the effect of the roughness on the flow after the step. Hence for simplicity there is no roughness in the inflow region prior to the step, and the roughness does not cover the full horizontal extent of the domain, simplifying both inflow and outflow conditions. In this case, both viscosity $\nu = 0.1$ and $\epsilon = 0.1$, and the horizontal length of the domain is $L = 23$. A Poiseuille inflow profile drives the flow, and the Reynolds number based on the profile is $Re = 150$. At this value, some recirculation after the step is expected. A zero-stress condition is applied at the outflow $x_1 = 23$: $\nabla u - pI = 0$, and for both the full DNS solution and the 1st order approximation,

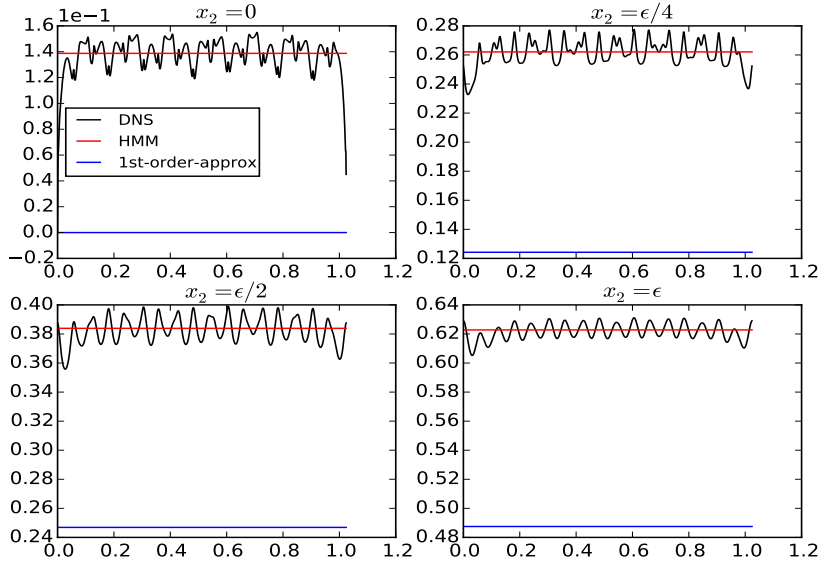


FIG. 12. Horizontal component of the flow u_1 versus x_1 plotted at various heights x_2 for the domain shown in [Figure 4d](#).

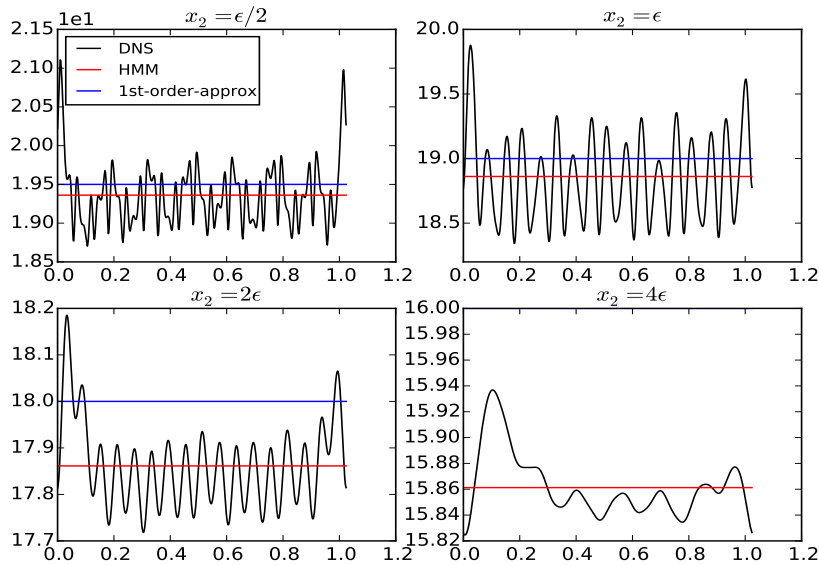


FIG. 13. Shear $\partial u_1 / \partial x_2$ versus x_1 plotted at various heights x_2 for the domain shown in [Figure 4d](#).

the no slip condition is applied on all other domain boundaries. The HMM solution, of course however satisfies the slip condition (4.3).

Algorithm 4.1 is used with two points $\{s_1, s_2\} = \{7.5, 13.5\}$ (marked with black dots in Figure 4e) chosen to lie (i) closer to the step, and hence within the recirculation bubble, and (ii) farther away from the step, after the bubble. Given $\{\alpha_1, \alpha_2\}$ at these micro domain locations, the slip amount is given as a piecewise linear interpolant

$$(5.10) \quad \alpha(x_1) = \mathbf{1}_{[6,16]}(x_1) \mathcal{I}_{\text{linear}}((6, 0), (7.5, \alpha_1), (13.5, \alpha_2), (16, 0))(x_1)$$

where $\mathbf{1}$ is the indicator function, and $x_1 = 6$ and $x_1 = 16$ are the points at which the roughness begins and ends, and hence before and after which there should be no slip. In retrospect a piecewise constant interpolant $\mathcal{I}_{\text{constant}}$ in the region $6 \leq x_1 \leq 16$ would be more appropriate, since (5.10) does not capture the slip amount as far out in x_1 as it should. Another option would be to simply perform micro simulations at more points $s_j \in [6, 16]$ along the roughness.

In this case the more general projection $\pi_j(U)$ is applied in both micro-domains. Because of the fluid recirculation, there is a nontrivial mass flux along the upper computational boundary $x_2 = 4\epsilon$ of the micro-domain at $s_1 = 7.5$. This results in a 10.2% difference in the slip amounts computed at $s_1 = 7.5$ and $s_2 = 13.5$. As a result, the HMM solution correctly captures the effect of roughness on the size of the recirculation bubble, something the 1st-order approximation fails to do. Figure 14 and Figure 15 illustrate the utility of constraining the micro-domains to match the local macroscopic solution.

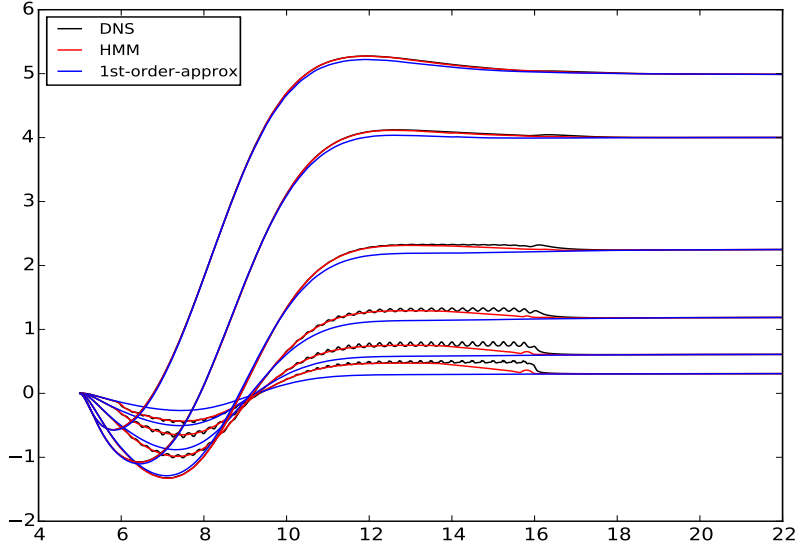


FIG. 14. Horizontal component of the flow u_1 versus x_1 plotted at the values $x_2 = \epsilon/4, \epsilon/2, \epsilon, 2\epsilon, 4\epsilon, 0.55$ for the domain shown in Figure 4e.

Acknowledgments. The authors acknowledge support from the Oden Institute for Computational Engineering and Sciences.

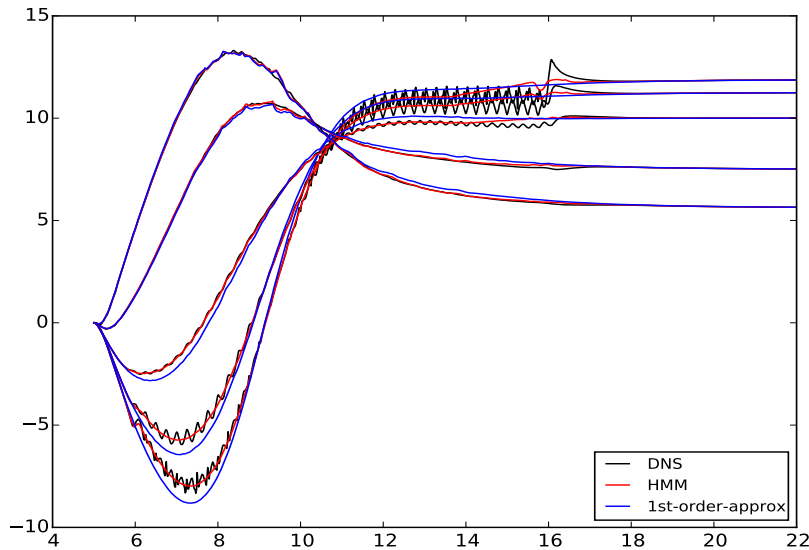


FIG. 15. Shear $\partial u_1/\partial x_2$ versus x_1 plotted at the values $x_2 = \epsilon/2, \epsilon, 2\epsilon, 4\epsilon, 0.55$ for the domain shown in Figure 4e.

- [1] A. ABDULLE, E. WEINAN, B. ENGQUIST, AND E. VANDEN-EIJNDEN, *The heterogeneous multiscale method*, Acta Numerica, 21 (2012), p. 187, <https://doi.org/10.1017/S0962492912000025>.
- [2] Y. ACHDOU, *Effet d'un mince revetement metallise mince sur la reflexion d'une onde electromagnetique*, C.R. Acad. Sci. Paris Ser. I, 314(3) (1992), pp. 217–222.
- [3] Y. ACHDOU AND O. PIRONNEAU, *Analysis of wall laws*, C.R. Acad. Sci. Paris Ser. I, 320 (1995), pp. 541–547.
- [4] Y. ACHDOU, O. PIRONNEAU, AND F. VALENTIN, *Effective boundary conditions for laminar flows over periodic rough boundaries*, J. Comput. Phys., 147(1) (1998), pp. 187–218.
- [5] Y. ACHDOU, P. L. TALLEC, F. VALENTIN, AND O. PIRONNEAU, *Constructing wall laws with domain decomposition or asymptotic expansion techniques*, Comput. Methods Appl. Mech. Engrg., 151 (1998), pp. 215–232.
- [6] Y. AMIRAT, O. BODART, U. D. MAIO, AND A. GAUDIELLO, *Effective boundary condition for stokes flow over a very rough surface*, Journal of Differential Equations, 254 (2013), pp. 3395 – 3430, <https://doi.org/http://dx.doi.org/10.1016/j.jde.2013.01.024>, <http://www.sciencedirect.com/science/article/pii/S0022039613000429>.
- [7] D. ARJMAND AND O. RUNBORG, *A time dependent approach for removing the cell boundary error in elliptic homogenization problems*, Journal of Computational Physics, 314 (2016), pp. 206 – 227, <https://doi.org/https://doi.org/10.1016/j.jcp.2016.03.009>, <http://www.sciencedirect.com/science/article/pii/S0021999116001601>.
- [8] M. ARTOLA AND M. CESSENAT, *Diffraction d'une onde electromagnetique par une couche composite mince accolée a un conducteur epais*, C.R. Acad. Sci. Paris Ser. I, 313 (1991), pp. 231–236.
- [9] A. BASSON AND D. GRARD-VARET, *Wall laws for fluid flows at a boundary with random roughness*, Communications on Pure and Applied Mathematics, 61, pp. 941–987, <https://doi.org/10.1002/cpa.20237>, <https://onlinelibrary.wiley.com/doi/abs/10.1002/cpa.20237>, <https://arxiv.org/abs/https://onlinelibrary.wiley.com/doi/pdf/10.1002/cpa.20237>.
- [10] D. BRESCH AND D. GÉRARD-VARET, *Roughness-induced effects on the quasi-geostrophic model*, Communications in Mathematical Physics, 253 (2005), pp. 81–119, <https://doi.org/10.1007/s00220-004-1173-9>, <https://doi.org/10.1007/s00220-004-1173-9>.
- [11] D. M. BUSHNELL AND K. J. MOORE, *Drag reduction in nature*, Annual Review of Fluid Mechanics, 23 (1991), pp. 65–79, <https://doi.org/10.1146/annurev.fl.23.010191.000433>.

- [12] A. CHORIN AND J. MARSDEN, *A Mathematical Introduction to Fluid Mechanics*, Springer-Verlag New York, 1993, <https://doi.org/10.1007/978-1-4612-0883-9>.
- [13] A.-L. DALIBARD AND D. GRARD-VARET, *Effective boundary condition at a rough surface starting from a slip condition*, *Journal of Differential Equations*, 251 (2011), pp. 3450 – 3487, <https://doi.org/http://dx.doi.org/10.1016/j.jde.2011.07.017>, <http://www.sciencedirect.com/science/article/pii/S0022039611002683>.
- [14] G. DEOLMI, W. DAHMEN, AND S. MLLER, *Effective boundary conditions: A general strategy and application to compressible flows over rough boundaries*, *Communications in Computational Physics*, 21 (2017), p. 358400, <https://doi.org/10.4208/cicp.OA-2016-0015>.
- [15] E. DUSSAN, *On the spreading of liquids on solid surfaces: Static and dynamic contact lines*, *Annu. Rev. Fluid Mech.*, 11 (1979), pp. 371–400.
- [16] W. E AND B. ENGQUIST, *The heterogeneous multiscale methods*, *Commun. Math. Sci.*, 1(1) (2003), pp. 87–132.
- [17] W. E, B. ENGQUIST, X. LI, W. REN, AND E. VANDEN-EIJNDEN, *Heterogeneous multiscale methods: A review*, *Commun. Comput. Phys.*, 2 (2007), pp. 367–450.
- [18] B. ENGQUIST AND Y.-H. TSAI, *Heterogeneous multiscale methods for stiff ordinary differential equations*, *Mathematics of Computation*, 74 (2005), pp. 1707–1742, <http://www.jstor.org/stable/4100207>.
- [19] E. FRIEDMANN, *The optimal shape of riblets in the viscous sublayer*, *J. Math. Fluid. Mech.*, 12.
- [20] E. FRIEDMANN AND T. RICHTER, *Optimal microstructures drag reducing mechanism of riblets*.
- [21] C. GEUZAIN AND J.-F. REMACLE, *Gmsh: A 3-d finite element mesh generator with built-in pre- and post-processing facilities*, *International Journal for Numerical Methods in Engineering*, 79 (2009), pp. 1309–1331, <https://doi.org/10.1002/nme.2579>, <https://onlinelibrary.wiley.com/doi/abs/10.1002/nme.2579>, <https://arxiv.org/abs/https://onlinelibrary.wiley.com/doi/pdf/10.1002/nme.2579>.
- [22] A. GLORIA, *Reduction of the resonance error. Part 1: Approximation of homogenized coefficients*, *Mathematical Models and Methods in Applied Sciences*, 21 (2011), pp. 1601–1630, <https://doi.org/10.1142/S0218202511005507>, <https://hal.inria.fr/inria-00457159>.
- [23] W. GRABOWSKI, *Coupling cloud processes with the large-scale dynamics using the cloud-resolving convection parameterization (crp)*, *J. Atmos. Sci.*, 58(9) (2001), pp. 978–997.
- [24] I. GROOMS AND A. J. MAJDA, *Efficient stochastic superparameterization for geophysical turbulence*, *Proceedings of the National Academy of Sciences*, 110 (2013), pp. 4464–4469, <https://doi.org/10.1073/pnas.1302548110>, <https://www.pnas.org/content/110/12/4464>, <https://arxiv.org/abs/https://www.pnas.org/content/110/12/4464.full.pdf>.
- [25] M. D. GUNZBURGER, *Finite Element Methods for Viscous Incompressible Flows: A Guide to Theory, Practice, and Algorithms*, Academic Press, 1989, <https://doi.org/https://doi.org/10.1016/C2009-0-22263-X>.
- [26] W. JÄGER AND A. MIKELIĆ, *On the interface boundary condition of beavers, joseph, and saffman*, *SIAM J. Appl. Math.*, 60(4) (2000), pp. 1111–1127.
- [27] W. JÄGER AND A. MIKELIĆ, *On the roughness-induced effective boundary conditions for an incompressible viscous flow*, *J. Differential Equations*, 170(1) (2001), pp. 96–122.
- [28] U. LĀCIS AND S. BAGHERI, *A framework for computing effective boundary conditions at the interface between free fluid and a porous medium*, *Journal of Fluid Mechanics*, 812 (2017), pp. 866–889.
- [29] W. LAYTON, *Introduction to the Numerical Analysis of Incompressible Viscous Flows*, Society for Industrial and Applied Mathematics, Philadelphia, PA, USA, 2008.
- [30] A. LOGG, K.-A. MARDAL, G. N. WELLS, ET AL., *Automated Solution of Differential Equations by the Finite Element Method*, Springer, 2012, <https://doi.org/10.1007/978-3-642-23099-8>.
- [31] A. LOGG, G. N. WELLS, AND J. HAKE, *DOLFIN: a C++/Python Finite Element Library*, Springer, 2012, ch. 10.
- [32] A. MAJDA, *Multiscale models with moisture and systematic strategies for superparameterization*, *J. Atmos. Sci.*, 64(7) (2007), pp. 2726–2734.
- [33] A. MAJDA AND M. GROTE, *Mathematical test models for superparameterization in anisotropic turbulence*, *PNAS*, 106(14) (2009), pp. 5470–5474.
- [34] A. J. MAJDA AND I. GROOMS, *New perspectives on superparameterization for geophysical turbulence*, *Journal of Computational Physics*, 271 (2014), pp. 60 – 77, <https://doi.org/https://doi.org/10.1016/j.jcp.2013.09.014>, <http://www.sciencedirect.com/science/article/pii/S0021999113006190>. *Frontiers in Computational Physics*.
- [35] A. MIKELIĆ, *Rough boundaries and wall laws*, (2009).
- [36] C. B. MILLIKAN, *A critical discussion of turbulent flows in channels and circular tubes*, in *Proceedings of the fifth International Congress for Applied Mechanics*, 1938, pp. 386–392.
- [37] J. PEDLOSKY, *Geophysical Fluid Dynamics*, Springer-Verlag New York, 1987, <https://doi.org/>

- [10.1007/978-1-4612-4650-3](https://doi.org/10.1007/978-1-4612-4650-3).
- [38] W. REN AND W. E, *Heterogeneous multiscale method for the modeling of complex fluids and microfluidics*, J. Comput. Phys., 204(1) (2005), pp. 1–26.
- [39] T. M. SQUIRES AND M. Z. BAZANT, *Induced-charge electro-osmosis*, Journal of Fluid Mechanics, 509 (2004), pp. 217–252.